Photochemistry and Photobiology, 2002, 75(4): 398–405

Monitoring Photoproduct Formation and Photobleaching by Fluorescence Spectroscopy Has the Potential to Improve PDT Dosimetry with a Verteporfin-like Photosensitizer¶

Haishan Zeng*[1], Mladen Korbelik[1], David I. McLean[2], Calum MacAulay[1] and Harvey Lui[2]

[1]Cancer Imaging Department, British Columbia Cancer Agency, Vancouver, BC, Canada and
[2]Division of Dermatology, Vancouver Hospital & Health Sciences Centre and University of British Columbia, Vancouver, BC, Canada

Received 20 August 2001; accepted 17 January 2002

ABSTRACT

In current clinical practice, photodynamic therapy (PDT) is carried out with prescribed drug doses and light doses as well as fixed drug–light intervals and illumination fluence rates. This approach can result in undesirable treatment outcomes of either overtreatment or undertreatment because of biological variations between different lesions and patients. In this study, we explore the possibility of improving PDT dosimetry by monitoring drug photobleaching and photoproduct formation. The study involved 60 mice receiving the same drug dose of a novel verteporfin-like photosensitizer, QLT0074, at 0.3 mg/kg body weight, followed by different light doses of 5, 10, 20, 30, 40 or 50 J/cm^2 at 686 nm and a fluence rate of 70 mW/cm^2. Photobleaching and photoproduct formation were measured simultaneously, using fluorescence spectroscopy. A ratio technique for data processing was introduced to reliably detect the photoproduct formed by PDT on mouse skin *in vivo*. The study showed that the QLT0074 photoproduct is stable and can be reliably quantified. Three new parameters, photoproduct score (PPS), photobleaching score (PBS) and percentage photobleaching score (PBS%), were introduced and tested together with the conventional dosimetry parameter, light dose, for performance on predicting PDT-induced outcome, skin necrosis. The statistical analysis of experimental results was performed with an ordinal logistic regression model. We demonstrated that both PPS and PBS improved the prediction of skin necrosis dramatically compared to light dose. PPS was identified as the best single parameter for predicting the PDT outcome.

INTRODUCTION

Photodynamic therapy (PDT) is a novel treatment modality for cancers as well as a variety of nononcologic applications (1–3). Although a degree of selectivity exists for PDT photosensitizers to localize to abnormal target tissue, normal cells or normal tissue (or both) are often still damaged during clinical PDT (4). Optimizing PDT dosimetry is crucial for ensuring adequate treatment of the disease, while at the same time minimizing damage to surrounding normal tissues.

Factors that affect the safety and efficacy of PDT include not only the photosensitizer drug and light doses, but also drug pharmacokinetics, drug and light distribution within the tissue and local oxygen supply (1). All the aforementioned factors are subject to significant biological variations amongst individual patients as well as different specific diseases and treatment sites. PDT dosimetry parameters derived from *in vitro* measurements, animal studies, theoretical modeling and prior empirical experience with other patients may not be sufficiently accurate for predicting the treatment response of a given patient. In current clinical practice, PDT is typically performed with prescribed drug doses and light doses as well as fixed drug–light intervals and illumination fluence rates, without specifically considering the biological variability of different treatment sites. Such an approach can sometimes result in one of two undesirable clinical outcomes: overtreatment caused by too much light irradiation of the treatment sites and undertreatment caused by insufficient light irradiation. Overtreatment may cause adverse effects such as strictures, fistulae, delayed healing, excessive scarring or cosmetic disfigurement, whereas in cases of undertreatment, the patients need to undergo additional PDT. During PDT it would be desirable to monitor the progress of therapy in real time and shut off the irradiation light when the optimum dose is reached. Such a system would require a measurable parameter that not only changes during therapeutic light exposure, but also correlates with the desired biological or clinical endpoints. Although various parameters have been proposed and evaluated for achieving rational ''biologic dosimetry'' including photosensitizer concentration, light distribution and oxygen concentration during PDT (1,4, 5–28), it is still technically difficult to directly monitor

¶Posted on the website on January 28, 2002.
*To whom correspondence should be addressed at: Cancer Imaging Department, British Columbia Cancer Agency, 601 West 10th Avenue, Vancouver, BC, Canada V5Z 1L3. Fax: 604-877-6077; e-mail: hzeng@bccancer.bc.ca

Abbreviations: BP, band pass; BPD-MA, benzoporphyrin derivative monoacid ring A; FCS, fetal calf serum; PBS, photobleaching score; PBS%, percentage photobleaching score; PDT, photodynamic therapy; PPS, photoproduct score; ROC, receiver operating characteristic.

singlet oxygen, which is the active mediator of PDT (29–31). A number of authors have suggested monitoring the decrease in photosensitizer fluorescence intensity caused by photobleaching or photoinactivation during light irradiation, under the assumption that this correlates with the local concentration of singlet oxygen, and by implication the treatment outcome (10,11, 32–35). Nevertheless, the potential reaccumulation of additional photosensitizer molecules at the treatment site during and after light exposure, caused by ongoing drug delivery *via* the peripheral circulation, can render photobleaching measurements inaccurate. Specifically, local reaccumulation of photosensitizer during light treatment may result in unexpectedly higher tissue drug effects than what would be predicted from simply measuring the decrease in fluorescence (or photobleaching) as a result of light exposure.

In addition and parallel to drug photobleaching during PDT, native photosensitizers can be photochemically converted to new species known as ''photoproducts'' (36–45). Photoproducts can exhibit measurable differences in their fluorescence properties as compared with those of their corresponding native photosensitizers, particularly in terms of maximum emission wavelength. Photoproduct levels may reflect the net photochemical effects of light and oxygen within tissue on native photosensitizers. The influence of any ongoing native photosensitizer delivery during light exposure is accounted for by the fact that any of the ''new'' photosensitizers that is also activated during the course of light exposure would contribute to the PDT effect as well as the total measurable photoproduct level.

Gillies *et al.* (45) reported a detailed study on the photophysical properties of a photoproduct generated *in vitro* from verteporfin (benzoporphyrin derivative monoacid ring A [BPD-MA]) in fetal calf serum (FCS) solutions under 694 nm light irradiation, and they suggested that quantifying this photoproduct fluorescence might provide a surrogate dosimeter for verteporfin-PDT effects. Iinuma *et al.* have observed the same photoproduct in cells and rat tumor models (46). However, there has been no report on utilizing photoproduct formation for clinical PDT dosimetry or systematic quantification and correlation of photoproduct fluorescence with biologic effects in animal models *in vivo*. By taking the ratio of fluorescence spectra measured during or after PDT light irradiation to spectra measured before light irradiation (H. Zeng, M. Korbelik, D. I. McLean, C. MacAulay, H. Liu), we have been able to detect a verteporfin photoproduct generated from PDT treatment of skin cancer and psoriasis *in vivo* (unpublished). This photoproduct is ordinarily difficult to discern from emission spectra alone. With this technique, we have also experimented with illuminating a skin site with verteporfin, using a 442 nm He–Cd laser and monitoring the photoproduct peak continuously during the illumination. We observed continuous increases of the photoproduct signal and no photobleaching of the photoproduct peak during illumination. In contrast, verteporfin photoproducts were not observed when verteporfin was irradiated in buffered saline solutions, homogeneous organic solutions or degassed FCS solutions (45), suggesting that verteporfin photoproduct formation is specific for biological systems supplied with oxygen and may therefore serve as an appropriate parameter or ''biological dosimeter'' for predicting biological effects

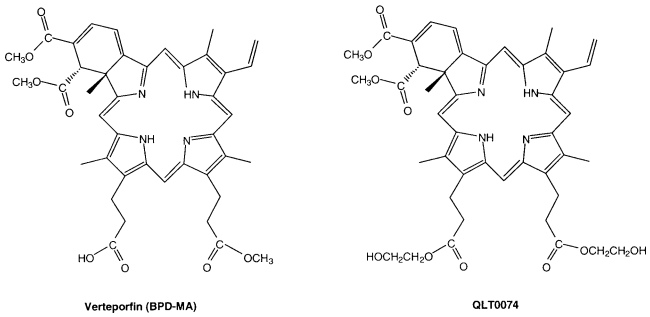

Figure 1. Chemical structures for BPD-MA and QLT0074.

and subsequent clinical outcome. Our hypothesis is that for certain types of photosensitizers, the photoproducts that are produced as a result of light exposure, presumably in proportion to the light–drug–oxygen interactions occurring within the tissue, can be used to monitor the net effective PDT dose, thereby predicting the eventual treatment outcome. Such photoproducts can be detected by various optical methods, and in this study, photoproducts that fluoresce are quantified *via* spectroscopy. To test this hypothesis, we designed experiments to examine the relationships between photoproduct formation, photobleaching and cutaneous responses in normal mouse skin, using a novel verteporfin-like photosensitizer, QLT0074.

MATERIALS AND METHODS

Photosensitizer. Although a number of drugs have shown photoproduct formation during PDT, not all their photoproducts are stable. For example, the 5-aminolaevulinic acid–related photoproduct from protoporphyrin IX can itself be photobleached by treatment light irradiation (36,47), and it is therefore not suitable for dosimetry studies without more complicated pharmacokinetic modeling. In this study, we used a novel verteporfin-like photosensitizer, QLT0074, which has photophysical properties similar to those of verteporfin but with a more rapid pharmacokinetic profile (Fig. 1; unpublished data, QLT Inc., Vancouver, BC, Canada) that is more convenient for animal experiments. With QLT0074, PDT treatment can be performed on mice 30 min after drug injection. The photosensitizer was supplied by QLT Inc. (batch QLA001) as a freeze-dried powder and reconstituted by the addition of sterile water to a concentration of 1.93 mg/mL. The photosensitizer was protected from light, stored at 4°C and used within 6 days after reconstitution.

Animals. BALB/c mice weighing 18–28 g (7–9 weeks old) were used in this study. They were fed a special diet (48) to eliminate chlorophyll-based tissue fluorescence, which peaks at 670 nm and interferes with both the photosensitizer and photoproduct signals. The study design was approved by the University of British Columbia Committee on Animal Care. The mice were immobilized without anesthesia in specially designed holders that exposed their backs. Hair on the lower back of the mice was shaved before PDT irradiation and optical measurements.

PDT treatment. QLT0074 was delivered by intravenous injection into the mice tail veins at a fixed dose of 0.3 mg/kg body weight. A diode laser (SDL, Inc., San Jose, CA; model 7422) tuned to 686 nm was used to irradiate the treatment skin site through an 8 mm diameter liquid light guide (Lumatec, Munchen, Germany; Series 2000). A special probe holder (Fig. 2) was designed to position the light guide perpendicular to the skin surface, while maintaining an illumination spot size of 10.5 mm diameter. The illumination power was kept at 60 mW, resulting in a fluence rate of 70 mW/cm^2. An electronic shutter (Vincent Associates, Rochester, NY; model VS25S1T1) controlled the light exposure time. Irradiation always commenced at 30 min after drug injection. PDT treatments were performed on 60 mice divided into six groups, with each group

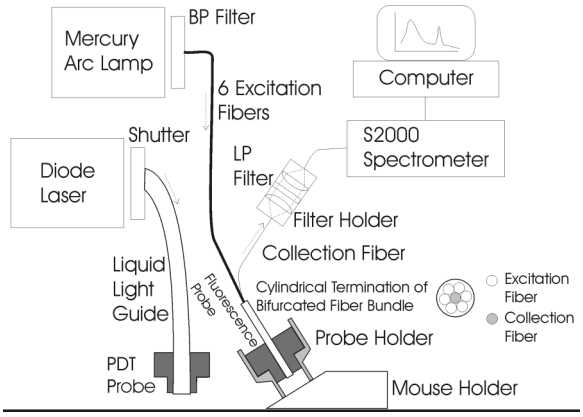

Figure 2. PDT treatment and fluorescence measurement system. The diode laser, the electrical shutter, the liquid light guide and the PDT probe form the treatment arm. The measurement arm consists of a mercury arc lamp, a BP filter, a bifurcated fiber probe, an inline filter holder and computer-controlled spectrometer. In this figure, the experimental setup depicted is configured for fluorescence measurement.

receiving one of six different light doses: 5, 10, 20, 30, 40 or 50 J/cm^2.

Assessment of skin reaction to PDT. Clinical observations of skin response were made serially on the first day and repeated every other day until 2 weeks after PDT treatment. The presence and degree of edema, erythema, purpura, blistering and necrosis were each scored from 0 to 3 (Table 1).

Fluorescence spectroscopy measurements of photoproducts and photobleaching. As with verteporfin, QLT0074 has a significant fluorescence emission peak around 695 nm when excited by shorter wavelength visible light. As a result of PDT treatment, it also generates photoproducts that fluoresce at around 650 nm when excited by the appropriate wavelengths of light. Blue light (437 nm) from a mercury arc lamp was used to excite both the photosensitizer and the photoproduct fluorescence so that both photoproducts and photobleaching could be monitored simultaneously. Figure 2 shows the spectrofluorometer configuration. A high-pressure mercury arc lamp (Oriel Instruments, Stratford, CT; model 60100) with a band pass (BP) filter (437 $\pm$ 10 nm; Omega Optical, Inc., Brattleboro, VT) provides excitation illumination through the six-fiber branch of a bifurcated fiber bundle. The six-fiber branch outputs about 8 mW of blue light and illuminates a 5 mm size spot at the center of the PDT treatment spot (10.5 mm in size). The central fiber at the distal end of the fiber bundle collects the fluorescence and transmits these photons to a computer-controlled spectrometer (Ocean Optics, Inc., Dunedin, FL; model S2000) for spectral analysis. A filter holder with a 475 nm long wave pass filter (Melles Griot, Irvine, CA; GG475) was used to block the reflected excitation light, while passing the longer wavelength fluorescence light. The acquisition of complete fluorescence emission spectra each took less than 1 s, and any PDT effect generated by the fluorescence excitation light was presumed to be minimal. The probe holder was mounted on an articulated arm and kept in gentle but complete contact with the mouse skin surface. The end of the probe holder had an inner diameter of 16 mm and an outer diameter of 24 mm. There is a pin inside the probe holder and corresponding notches on the fluorescence and PDT probes to make sure that both probes remain in exactly the same relative position inside the holder.

The experimental procedure for each animal was as follows. First, the mouse was immobilized in the special holder, and the native fluorescence spectrum of the mouse skin site to be treated was measured. The mouse then received the intravenous injection of QLT0074. Thirty minutes after drug injection, a pretreatment fluorescence spectrum was measured and denoted as $I_0(\lambda)$, with λ being the wavelength of the emitted light. The fluorescence probe was taken out of the probe holder and replaced by the PDT probe to initiate the PDT treatment irradiation, which took t minutes. Immediately after PDT treatment, the fluorescence probe was exchanged for the PDT probe, and an aftertreatment fluorescence spectrum was measured and denoted as $I_t(\lambda)$.

Figure 3 shows example spectra serially obtained from a mouse treated with 20 J/cm^2 of 686 nm laser light over 4.8 min. Figure 3a shows the native skin fluorescence spectrum before drug injection, the fluorescence spectrum 30 min after drug injection but right before PDT treatment and the fluorescence spectrum right after PDT treatment. To assess the photoproduct stability after PDT light irradiation, fluorescence spectra were also measured 6 min after the termination of PDT treatment. Native skin autofluorescence peaks around 510 nm, and the QLT0074 fluorescence signal peaks around 695 nm, whereas the photoproduct signal appears around 650 nm. The decrease in drug fluorescence signal around 695 nm as a result of PDT light irradiation can be readily seen and reflected drug photobleaching. PDT light irradiation also resulted in a fluorescence signal increase around 650 nm because of photoproduct formation (45). Six minutes after PDT treatment, the drug fluorescence signal increased, confirming that drug reaccumulation can affect the accuracy of photobleaching measurements. The photoproduct signal appeared quite stable for at least 6 min after PDT treatment. Figure 3b shows fluorescence ratio spectra generated by taking each emission spectra after PDT and dividing it by the same spectrum taken immediately before PDT treatment. The 650 nm photoproduct peak is more apparent on this graph and remains almost constant after the termination of PDT light treatment at the final 6 min measurement time. In the autofluorescence range (480–620 nm) and the native drug fluorescence range (670–750 nm), there are appreciable differences between the two curves. Immediately after PDT treatment, the

Table 1. Scoring system for assessment of skin reaction to PDT

Severity/score	Edema	Erythema*	Purpura	Vesicle/blister	Necrosis
Absent/0	None	None	None	None	None
Minimal/1	Minimally perceptible edema within exposure site	Minimally perceptible erythema at field of exposure, above baseline	Minimal haemorrhage, area of purpura is smaller than exposure site	Minimal area of vesicle/blister (<50% of exposure site)	Very superficial, smaller area (relative to light exposure area) white–pink crust
Moderate/2	Skin fold up to 1 mm thickness within exposure site	Moderate erythema	Mild to moderate purpura above baseline: fine petechiae	Larger area vesicle/blister (>50% of exposure site)	Superficial large area (relative to light exposure area) pink–red crust
Severe/3	1–2 mm thickness of skin fold	Erythema associated with edema	Severe purpura: patchy or large areas of purpura	Erosion vesicles or blisters	Dark-brown thick scab within exposure site

*When pressure is applied, mild or moderate erythema is blanchable as compared to purpura, which is not.

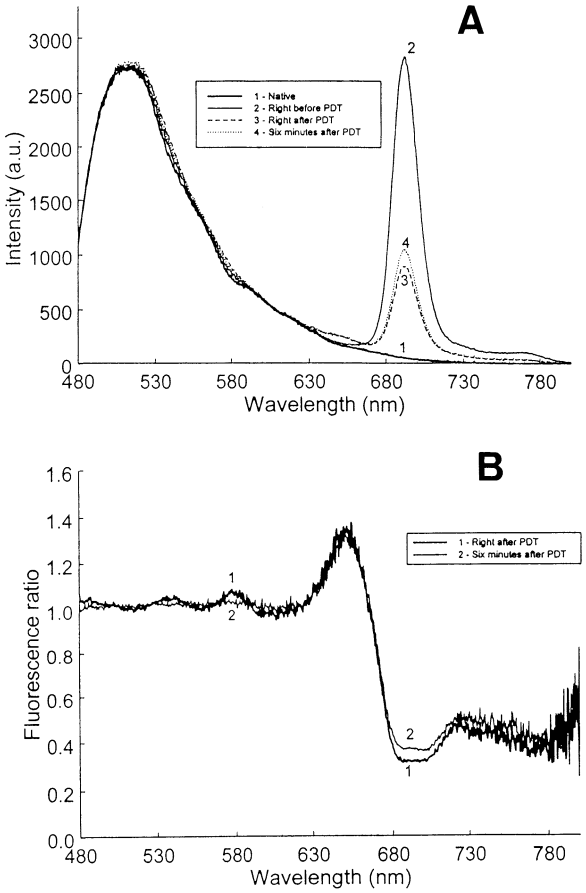

Figure 3. Example fluorescence spectra. (a) The native skin spectrum before drug injection and the spectra before and after PDT treatment. (b) Fluorescence ratio spectra generated by taking the spectra after PDT and dividing it by the spectrum taken before PDT.

fluorescence ratio showed two peaks at 540 and 580 nm, indicating the effect of decreased blood flow, blood vessel shutdown or hemoglobin oxygenation changes (or both). Six minutes after PDT, the ratio curve becomes flatter at the 540 and 580 nm wavelengths, indicating restoration of normal blood content or tissue oxygenation at the treatment site (49). This restoration correlated with photosensitizer replenishment as evidenced by increased fluorescence at 670–750 nm.

Integration of the photoproduct peak (around 650 nm) on the ratio curve (Fig. 3b) was used to quantify photoproducts generated during PDT treatment, and the integral was defined as the photoproduct score (PPS).

$$\mathrm{PPS} = \int_{620\ \mathrm{nm}}^{670\ \mathrm{nm}} [\mathrm{I_t}(\lambda)/\mathrm{I_0}(\lambda)]\ d\lambda. \qquad (1)$$

The apparent amount of photosensitizer being photobleached should be proportional to the integral of $(I_0 - I_t)$ around the photosensitizer fluorescence peak (695 nm), assuming that photosensitizer replenishment during PDT treatment is neglected, and this quantity is defined as the photobleaching score (PBS).

$$\mathrm{PBS} = \int_{670\ \mathrm{nm}}^{750\ \mathrm{nm}} [\mathrm{I_0}(\lambda) - \mathrm{I_t}(\lambda)]\ d\lambda. \qquad (2)$$

The relative amount of photobleaching can also be calculated as the percentage of photosensitizer photobleached (percentage photobleaching score [PBS%]).

$$\mathrm{PBS\%} = \int_{670\ \mathrm{nm}}^{750\ \mathrm{nm}} [\mathrm{I_0}(\lambda) - \mathrm{I_t}(\lambda)]\ d\lambda \Big/ \int_{670\ \mathrm{nm}}^{750\ \mathrm{nm}} \mathrm{I_0}(\lambda)\ d\lambda. \qquad (3)$$

The right-hand sides of Eqs. 2 and 3 do not necessarily represent the exact quantity of photosensitizer that has been photobleached if photosensitizer replenishment occurs during the PDT treatment, which is likely the case with QLT0074 in the experimental setting tested. In this situation the calculated value is always smaller than the actual amount of photosensitizer photobleached. In contrast, the right-hand side of Eq. 1 should describe the actual amount of photoproducts generated, regardless of how much photosensitizer reaccumulation has occurred during PDT. The effect of any new photosensitizer delivered to the treatment site during light exposure, which is also photoactivated, will be reflected in the photoproduct calculated from Eq. 1.

Another important consideration is that $(I_0 - I_t)$ depends on the detection efficiency, which in turn is influenced by the fluorescence measurement geometry. The probe holder was designed to maintain constant measurement geometry among different mice or at different measurement times. The intensity of the excitation light as well as the exposure time of the spectrometer charge coupled device were recorded and used to normalize the spectra collected. In contrast, the (I_t/I_0) ratio calculation cancels the dependence of PPS on the excitation light intensity and the detection efficiency, and thus PPS could be more accurately quantified than PBS.

Statistical analysis. Because the observed outcomes, *i.e.* skin responses to PDT, were ordered categorical variables (*i.e.* 0, 1, 2 and 3), an ordinal logistic regression model was used to analyze the effects of various dosimetry parameters (light dose, PPS, PBS and PBS%) on skin responses (edema, erythema, purpura, blistering and necrosis). The PR program in the BMDP Package (BMDP Statistical Software, Inc., Los Angeles, CA) was used for the analysis. This program systematically examines the dosimetry parameters in a stepwise manner and determines which dosimetry parameters will best predict the observed outcomes. Goodness-of-fit tests in the program indicate the degree of success of the model prediction. Usually, a goodness-of-fit *P* value above 0.5 indicates an acceptable fit of the model to the data. For more details of this model, see Refs. (50–53).

To further evaluate the model for predicting the treatment outcomes, the skin responses were regrouped into dichotomous categories: {0 and 1} *versus* {2 and 3}. Regular logistic regression was performed to generate a classification table, showing correct and incorrect classifications for the dichotomous categories (''absent or minimal response'' *vs* ''moderate to severe response'') (54) at different threshold levels, and using these results, receiver operating characteristic (ROC) plots were generated. An ROC plot is obtained by plotting all true positive fractions on the *y*-axis against their equivalent false positive fractions for all available thresholds on the *x*-axis. The closer the curve to the upper left corner, the better the classification performance.

RESULTS

Overall description of experimental data

Of the five types of skin responses (edema, erythema, purpura, blistering and necrosis) evaluated, only edema and necrosis showed three or more different categories of scores with relatively even distributions among different categories for all 60 mice, thereby warranting meaningful data analysis. The maximum values of edema or necrosis scored during the 2 week observation period were used as the final scores for data analysis. Although edema is observable shortly after PDT treatment, necrosis is a more important and clinically relevant tissue effect because all other observable effects, including edema, resolve without permanent sequelae (*i.e.* scarring). Detailed data will therefore be shown only for necrosis. Moreover, there appeared to be a correlation between the extents of necrosis and edema, and the overall analysis showed similar results (data not shown).

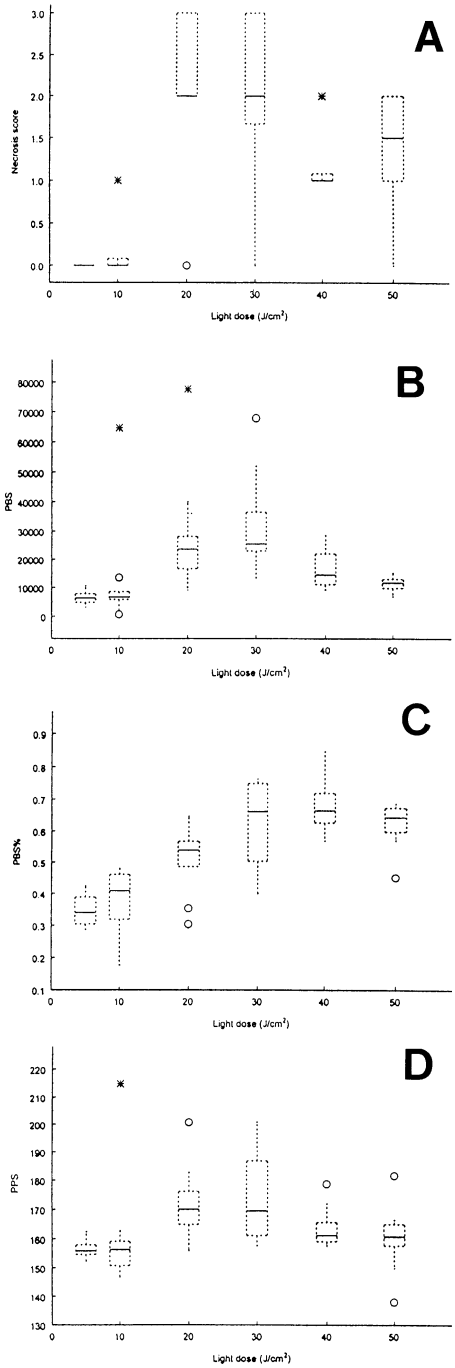

Figure 4. Box plots of skin necrosis, PBS, PBS% and PPS at different light doses. (a) Necrosis; (b) PBS; (c) PBS%; and (d) PPS. In these box plots, the solid horizontal line represents the median value, whereas the box indicates the interquartile range (25th–75th percentiles). The width of the box is proportional to the square root of the number of data points in each group (they are all 10 in this graph). The length of the vertical line on each end of the box is determined by the ''step,'' which equals 1.5 times the height of the box. The upper vertical line extends up to the highest value in the data within the step, and the lower vertical line extends down to the lowest value in the data within the step. The * symbol denotes outer data points that are larger than (median + 3 times the height of the box) or smaller than (median − 3 times the height of the box). The ° symbol denotes data points that are inside the outer symbol range, but outside the range of (median + 1.5 times the height of the box) and (median − 1.5 times the height of the box).

Distribution of skin response scores, PPS, PBS and PBS% between treatment groups

Figure 4 shows the box plots for necrosis, PBS, PBS% and PPS as functions of PDT light doses. Within each light dose group, the skin responses varied significantly. Furthermore, for different groups, higher light doses did not necessarily result in higher degrees of necrosis. PBS, PBS% and PPS values also showed large variations within each mouse group that received the same light dose. Of necrosis, PBS, PBS% and PPS, only PBS% appeared to demonstrate some correlation with light dose ($R = 0.752$ by linear regression).

Correlations between skin responses and dosimetry parameters analyzed on an individual mouse basis

Because even with the same drug dose and light doses administrated, different mice had very different skin responses as well as photoproduct and photobleaching parameters, it is important to analyze the data on an individual mouse basis rather than by light dose groups. In Fig. 5 are separate box plots of light dose, PBS, PBS% and PPS *versus* necrosis score. Figure 5a,c shows poor correlations for light doses and PBS% with the necrosis scores. Figure 5b,d suggests that PBS and PPS may each correlate well with skin necrosis.

To determine which of the four dosimetry parameters (light dose, PPS, PBS and PBS%) can best predict the PDT treatment outcome of skin necrosis, an ordinal logistic regression model was developed, using the four dosimetry parameters as independent variables and necrosis score as the dependent variable. Stepwise analysis results suggest that PPS is the best single parameter for predicting skin necrosis with a goodness-of-fit P value of 0.973. This seems consistent with Fig. 5 showing more outer data points in Fig. 5b for PBS than in Fig. 5d for PPS. If two parameters were used to predict necrosis, PPS and light dose are the best combination, with a slightly improved goodness-of-fit P value = 0.995. After step 2, no additional independent variables could be added in the stepwise process to further improve the model fit. In contrast, if light dose alone is applied to the model as a single independent parameter, the goodness-of-fit P value is less than 0.001.

ROC for model prediction of PDT treatment outcomes

The performance of the regression model was further tested by regrouping the necrosis scored into dichotomous categories: {0 and 1} for absent or minimal necrosis, and {2 and 3} for moderate to severe necrosis. Regular logistic regression was then performed to generate an ROC plot in terms of the above dichotomous categories. The optimized single dosimetry parameter, PPS, from the ordinal logistic regression was applied to the model to generate the ROC curve. For comparison, ROC curves were also obtained by applying light dose alone or PBS% alone as the only independent variables for the model. From the ROC curves shown in Fig. 6, PPS is closer to the upper left corner and therefore better predicts PDT outcome in terms of necrosis than does light dose alone or PBS% alone.

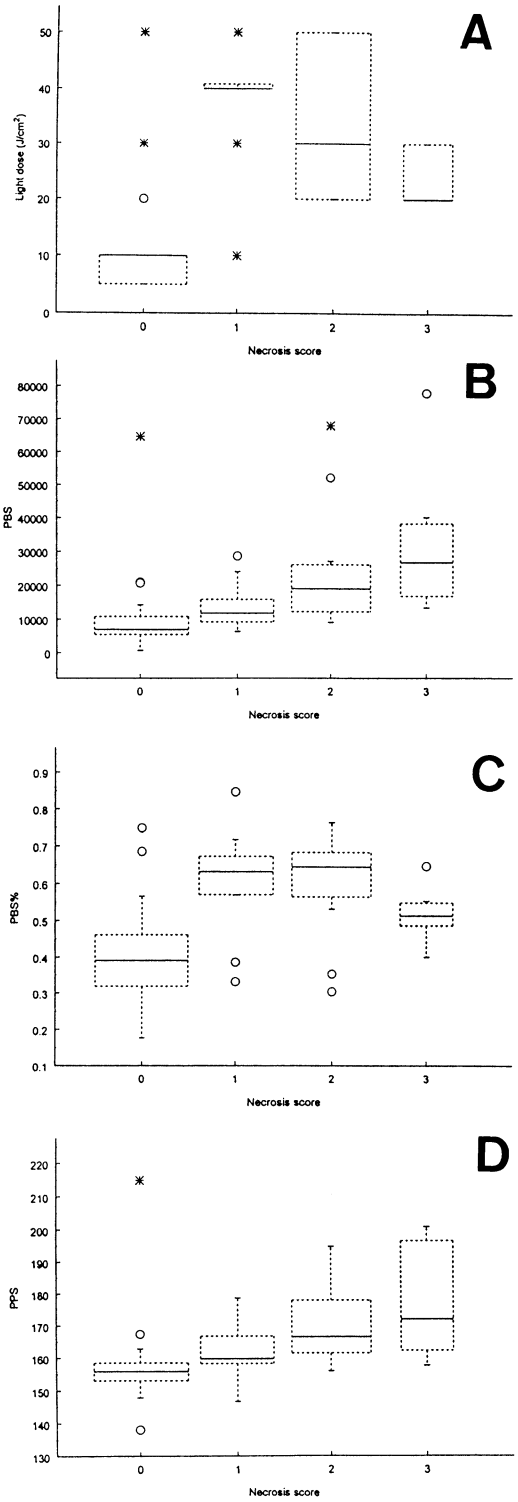

Figure 5. Box plots of light dose, PBS, PBS% and PPS *versus* necrosis score. (a) Light dose; (b) PBS; (c) PBS%; and (d) PPS. Here, all the legends have the same meanings as in Fig. 4. Again, the width of the box is proportional to the number of cases in each necrosis category (22 cases for score 0, 14 cases for score 1, 16 cases for score 2 and 7 cases for score 3).

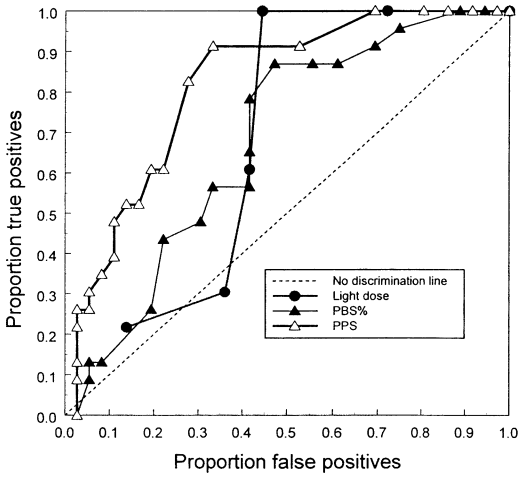

Figure 6. ROC of model prediction of PDT treatment outcomes. PPS is significantly better for predicting PDT-induced necrosis than light dose.

DISCUSSION

In this study we evaluated a range of optical parameters and their derivatives for noninvasive *in vivo* monitoring of PDT effects. A normal mouse skin model was used to evaluate necrosis, which is a clinically relevant endpoint because of its association with significant irreversible tissue damage and scarring. We have demonstrated that a PDT drug photoproduct can be reliably measured *in vivo* from mouse skin, using fluorescence spectroscopy and a ratio data processing technique (Fig. 3b). The measured photoproduct was stable and was not carried away by blood circulation because its fluorescence signal did not change for at least several minutes after PDT irradiation was terminated. Under the PDT conditions in our experiments, photosensitizer reaccumulation presumably occurs because of blood circulation and is evident in Fig. 3. The photosensitizer fluorescence signal at 695 nm increased within 6 min after PDT irradiation. Such drug reaccumulation results in the measured PBS underestimating the actual photobleaching that has occurred during PDT. The overall effect of drug reaccumulation is potentially even greater for PDT protocols that employ fractionated light dose regimens.

Our results showed that there can be a poor correlation between light dose and skin necrosis, suggesting a need for utilizing additional or different parameters (or both) for guiding PDT dosimetry. Despite our clinical experience and the variability shown in the experimental results, clinical PDT dosimetry continues to be more or less empirically based on prescribed doses of drug and light. Of the three parameters (PPS, PBS and PBS%) evaluated, PBS% showed poor correlation with skin necrosis, although it correlated, to some extent, with light dose ($R = 0.752$). Both PBS and PPS showed good correlation with skin necrosis. PBS% measures relative photosensitizer photobleaching by PDT light irradiation. At a fixed irradiance, the longer the light exposure time, the higher the fraction of photosensitizer that is photobleached. This relative score seems to be independent of the amount of photosensitizer present at the treatment site. Thus, PBS% is nearly proportional to the light dose and also independent of biological variability between different

treatment sites and animals. Our observation is consistent with previous work by Iinuma *et al.* (46), which demonstrated that verteporfin photobleaching in a rat tumor followed an exponential function, e^{-kD}, where k is a constant in the order of 0.01, and D is light dose in units of J/cm^2. At lower light doses, PBS% is equivalent to $1 - e^{-kD} \approx 1 - (1 - kD) = kD$, and therefore PBS% is proportional to light dose. In contrast, at higher light doses, we observed a plateau in the PBS% *versus* light dose relationship in Fig. 4c, which may be the result of the effect of photosensitizer reaccumulation because PDT treatment times were longer with higher light doses, thereby allowing more drug reaccumulation, which in turn would result in an apparent lowering of the overall measurable photobleaching. Another possible reason is that at higher light doses, more vascular damage will lead to less oxygen supply and correspondingly less photobleaching of the photosensitizer for oxygen-dependent photobleaching.

PBS measures the absolute amount of photosensitizer that is photobleached and may be dependent on the amount of photosensitizer present at the treatment site and the rate of reaction between light, drug and oxygen. Therefore, PBS shows poor correlation with light dose alone because of biological variations between different treatment sites and animals. Although correlated with each other, PBS% and light dose are not interchangeable parameters; for example, our results show that PBS% is the best single parameter for predicting skin edema but not necrosis (data not shown). The combination of PPS and light dose represents the best parameter for predicting skin necrosis when two parameters were used in our model.

The correlation of PPS and PBS ($R = 0.806$) conforms to our results, showing that both were better at predicting PDT outcomes than light dose alone. Both PBS and PPS are related to drug photodegradation, which may be oxygen-dependent. Nevertheless, unlike photobleaching, photoproduct formation from verteporfin seems to occur only in the presence of proteins or lipoproteins (or both) at FCS or cellular targets in tissue (45), and this is presumably the same for QLT0074. As previously discussed, PPS can be more accurately estimated than PBS. These similarities and differences between PPS and PBS may explain their partial correlation with each other, as well as their differences in predicting skin necrosis. One explanation for why PPS was better at predicting the biological outcome is that photoproduct only forms at the biological targets. Indeed, our results demonstrated that PPS is the best single parameter for predicting PDT-induced necrosis. Although the results of this study need to be confirmed in humans, these results suggest that a clinically relevant form of PDT dosimetry for this class of drug could involve monitoring PPS in real time during PDT treatment. Individual light treatments would be stopped by shutting off the light instantly at predetermined optimal levels of PPS.

Acknowledgements—This work was supported by grants from the Canadian Dermatology Foundation and Biomax Technologies Inc. The photosensitizer, QLT0074, was provided by QLT Inc. We thank Mr. J. Sun and Ms. D. Hwang for their excellent technical assistance to the study, Dr. Michael Schulzer and Mr. Edwin Mak of the University of British Columbia Department of Medicine for statistical analysis, Dr. A. Doudkine and Ms. J. Wang of Biomax for assistance with data preprocessing and Dr. R. Boch of QLT for his advice on the photosensitizer.

REFERENCES

1. Dougherty, T. J., C. J. Gomer, B. W. Henderson, G. Jori, D. Kessel, M. Korbelik, J. Moan and Q. Peng (1998) Photodynamic therapy. *J. Natl. Cancer Inst.* **90**, 889–905.
2. Carruth, J. A. (1998) Clinical applications of photodynamic therapy. *Int. J. Clin. Pract.* **52**, 39–42.
3. Bissonnette, R. and H. Lui (1997) Current status of photodynamic therapy in dermatology. *Dermatol. Clin.* **15**, 507–519.
4. Bays, R., G. Wagnieres, D. Robert, D. Braichotte, J. F. Savary, P. Monnier and H. van den Bergh (1997) Light dosimetry for photodynamic therapy in the esophagus. *Lasers Surg. Med.* **20**, 290–303.
5. Murrer, L. H., H. P. Marijnissen and W. M. Star (1998) Monte Carlo simulations for endobronchial photodynamic therapy: the influence of variations in optical and geometrical properties and of realistic and eccentric light sources. *Lasers Surg. Med.* **22**, 193–206.
6. Glanzmann, T., C. Hadjur, M. Zellweger, P. Grosiean, M. Forrer, J. P. Ballini, P. Monnier, H. van den Bergh, C. K. Lim and G. Wagnieres (1996) Pharmacokinetics of tetra(*m*-hydroxyphenyl)chlorin in human plasma and individualized light dosimetry in photodynamic therapy. *Photochem. Photobiol.* **67**, 596–602.
7. Barajas, O., A. M. Ballangrud, G. G. Miller, R. B. Moore and J. Tulip (1997) Monte Carlo modeling of angular radiance in tissue phantoms and human prostate: PDT light dosimetry. *Phys. Med. Biol.* **42**, 1675–1687.
8. Tsoukas, M. M., G. C. Lin, M. S. Lee, R. R. Anderson and N. Kollias (1997) Predictive dosimetry for threshold phototoxicity in photodynamic therapy on normal skin: red wavelengths produce more extensive damage than blue at equal threshold doses. *J. Investig. Dermatol.* **108**, 501–505.
9. Chen, Q., B. C. Wilson, S. D. Shetty, M. S. Patterson, J. C. Cerny and F. W. Hetzel (1997) Changes in *in vivo* optical properties and light distributions in normal canine prostate during photodynamic therapy. *Radiat. Res.* **147**, 86–91.
10. Grossweiner, L. I. (1997) PDT light dosimetry revisited. *J. Photochem. Photobiol. B: Biol.* **38**, 258–268.
11. Svaasand, L. O., P. Wyss, M. T. Wyss, Y. Tadir, B. J. Tromberg and M. W. Berns (1996) Dosimetry model for photodynamic therapy with topically administered photosensitizers. *Lasers Surg. Med.* **18**, 139–149.
12. Beyer, W. (1996) Systems for light application and dosimetry in photodynamic therapy. *J. Photochem. Photobiol. B: Biol.* **36**, 153–156.
13. Janssen, W. G. (1996) Photodynamic therapy: a guide to instrumentation and dosimetry calculations. *Minim. Invasive Surg. Nurs.* **10**, 105–108.
14. Braichotte, D. R., J. F. Savary, P. Monnier and H. E. van den Bergh (1996) Optimizing light dosimetry in photodynamic therapy of early stage carcinomas of the esophagus using fluorescence spectroscopy. *Lasers Surg. Med.* **19**, 340–346.
15. Marijnissen, J. P. and W. M. Star (1996) Calibration of isotropic light dosimetry probes based on scattering bulbs in clear media. *Phys. Med. Biol.* **41**, 1191–1208.
16. Tromberg, B. J., L. O. Svaasand, M. K. Fehr, S. J. Madsen, P. Wyss, B. Sansone and Y. Tadir (1996) A mathematical model for light dosimetry in photodynamic destruction of human endometrium. *Phys. Med. Biol.* **41**, 223–237.
17. van Staveren, H. J., M. Keijzer, T. Keesmaat, H. Jansen, W. J. Kirkel, J. F. Beek and W. M. Star (1996) Integrating sphere effect in whole-bladder wall photodynamic therapy: III. Fluence multiplication, optical penetration and light distribution with an eccentric source for human bladder optical properties. *Phys. Med. Biol.* **41**, 579–590.
18. Messmann, H., P. Mlkvy, G. Buonaccorsi, C. L. Davies, A. J. MacRobert and S. G. Bown (1995) Enhancement of photodynamic therapy with 5-aminolaevulinic acid-induced porphyrin photosensitization in normal rat colon by threshold and light fractionation studies. *Br. J. Cancer* **72**, 589–594.
19. Murrer, L. H., J. P. Marijnissen and W. M. Star (1995) Ex vivo

light dosimetry and Monte Carlo simulations for endobronchial photodynamic therapy. *Phys. Med. Biol.* **40**, 1807–1817.
20. Heier, S. K., K. A. Rothman, L. M. Heier and W. S. Rosenthal (1995) Photodynamic therapy for obstructing esophageal cancer: light dosimetry and randomized comparison with Nd:YAG laser therapy. *Gastroenterology* **109**, 63–72.
21. Chen, Q., B. C. Wilson, M. O. Dereski, M. S. Patterson, M. Chopp and F. W. Hetzel (1992) Effects of light beam size on fluence distribution and depth of necrosis in superficially applied photodynamic therapy of normal rat brain. *Photochem. Photobiol.* **56**, 379–384.
22. Chen, Q., M. Chopp, M. O. Dereski, B. C. Wilson, M. S. Patterson, A. Schreiber and F. W. Hetzel (1992) The effect of light fluence rate in photodynamic therapy of normal rat brain. *Radiat. Res.* **132**, 120–123.
23. Wilson, B. C. (1989) Photodynamic therapy: light delivery and dosage for second-generation photosensitizers. *Ciba Found. Symp.* **146**, 60–77.
24. Muller, P. J. and B. C. Wilson (1987) Photodynamic therapy of malignant primary brain tumours: clinical effects, post-operative ICP, and light penetration of the brain. *Photochem. Photobiol.* **46**, 929–935.
25. Wilson, B. C., P. J. Muller and J. C. Yanch (1986) Instrumentation and light dosimetry for intra-operative photodynamic therapy (PDT) of malignant brain tumours. *Phys. Med. Biol.* **31**, 125–133.
26. Wilson, B. C. and M. S. Patterson (1986) The physics of photodynamic therapy. *Phys. Med. Biol.* **31**, 327–360.
27. Biolo, R., G. Jori, J. C. Kennedy, P. Nadeau, R. Pottier, E. Reddi and G. Weagle (1991) A comparison of fluorescence methods used in the pharmacokinetic studies of Zn(II)phthalocyanine in mice. *Photochem. Photobiol.* **53**, 113–118.
28. Pottier, R. (1990) *In vitro* and *in vivo* fluorescence monitoring of photosensitizers. *J. Photochem. Photobiol. B: Biol.* **6**, 103–109.
29. Parker, J. G. (1986) Optical detection of the photodynamic production of singlet oxygen *in vivo*. *Lasers Surg. Med.* **6**, 258–259.
30. Patterson, M. S., S. J. Madsen and B. C. Wilson (1990) Experimental tests of the feasibility of singlet oxygen luminescence monitoring *in vivo* during photodynamic therapy. *J. Photochem. Photobiol. B: Biol.* **5**, 69–84.
31. Niedre, M., M. S. Patterson and B. C. Wilson (2002) Direct near-infrared luminescence detection of singlet oxygen generated by photodynamic therapy in cells *in vitro* and tissues *in vivo*. *Photochem. Photobiol.* (In press)
32. Jongen, A. J. and H. J. Sterenborg (1997) Mathematical description of photobleaching *in vivo* describing the influence of tissue optics on measured fluorescence signals. *Phys. Med. Biol.* **42**, 1701–1716.
33. Georgakoudi, I., M. G. Nichols, T. H. Foster (1997) The mechanism of Photofrin photobleaching and its consequences for photodynamic dosimetry. *Photochem. Photobiol.* **65**, 135–144.
34. Rhodes, L. E., M. M. Tsoukas, R. R. Anderson and N. Kollias (1997) Iontophoretic delivery of ALA provides a quantitative model for ALA pharmacokinetics and PpIX phototoxicity in human skin. *J. Investig. Dermatol.* **108**, 87–91.
35. Grossweiner, L. I. (1986) Optical dosimetry in photodynamic therapy. *Lasers Surg. Med.* **6**, 462–466.
36. Robinson, D. J., H. S. de Bruijn, N. van der Veen, M. R. Stringer, S. B. Brown and W. M. Star (1998) Fluorescence photobleaching of ALA-induced protoporphyrin IX during photodynamic therapy of normal hairless mouse skin: the effect of light dose and irradiance and the resulting biological effect. *Photochem. Photobiol.* **67**, 140–149.
37. Rotomskis, R., S. Bagdonas and G. Streckyte (1996) Spectroscopic studies of photobleaching and photoproduct formation of porphyrins used in tumour therapy. *J. Photochem. Photobiol. B: Biol.* **33**, 61–67.
38. Gudgin Dickson, E. F. and R. H. Pottier (1995) On the role of protoporphyrin IX photoproducts in photodynamic therapy. *J. Photochem. Photobiol. B: Biol.* **29**, 91–93.
39. van Leengoed, H. L., V. Cuomo, A. A. Versteeg, N. van der Veen, G. Jori and W. M. Star (1994) *In vivo* fluorescence and photodynamic activity of zinc phthalocyanine administered in liposomes. *Br. J. Cancer* **69**, 840–845.
40. Castell, J. V., M. J. Gomez-Lechon, C. Grassa, L. A. Martinez, M. A. Miranda and P. Tarrega (1994) Photodynamic lipid peroxidation by the photosensitizing nonsteroidal antiinflammatory drugs suprofen and tiaprofenic acid. *Photochem. Photobiol.* **59**, 35–39.
41. Orth, K., K. Konig, F. Genze and A. Ruck (1994) Photodynamic therapy of experimental colonic tumours with 5-aminolevulinic-acid-induced endogenous porphyrins. *J. Cancer Res. Clin. Oncol.* **120**, 657–661.
42. Konig, K., H. Schneckenburger, A. Ruck and R. Steiner (1993) *In vivo* photoproduct formation during PDT with ALA-induced endogenous porphyrins. *J. Photochem. Photobiol. B: Biol.* **18**, 287–290.
43. Konig, K., H. Wabnitz and W. Dietel (1990) Variation in the fluorescence decay properties of haematoporphyrin derivative during its conversion to photoproducts. *J. Photochem. Photobiol. B: Biol.* **8**, 103–111.
44. Amit, I., Z. Malik and D. Kessel (1999) Photoproduct formation from a zinc benzochlorin iminium salt detected by fluorescence microscopy. *Photochem. Photobiol.* **69**, 700–702.
45. Gillies, R., N. Kollias, T. Hasan and H. Diddens (1996) Spectral characterization of the benzoporphyrin derivative monoacid ring—a photoproduct formed in fetal calf solutions during irradiation with 694 nm continuous-wave radiation. *J. Photochem. Photobiol. B: Biol.* **33**, 87–90.
46. Iinuma, S., K. T. Schomacker, G. Wagnieres, M. Rajadhyaksha, M. Bamberg, T. Momma and T. Hasan (1999) *In vivo* fluence rate and fractionation effects on tumor response and photobleaching: photodynamic therapy with two photosensitizers in an orthotopic rat tumor model. *Cancer Res.* **59**, 6164–6170.
47. Finlay, J. C., D. L. Conover, E. L. Hull and T. H. Foster (2001) Porphyrin bleaching and PDT-induced spectral changes are irradiance dependent in ALA-sensitized normal rat skin *in vivo*. *Photochem. Photobiol.* **73**, 54–63.
48. Holmes, H., J. C. Kennedy, R. Pottier, F. Rossi and G. Weagle (1995) A recipe for the preparation of a rodent food that eliminates chlorophyll-based tissue fluorescence. *J. Photochem. Photobiol. B: Biol.* **29**, 199.
49. Korbelik, M., C. S. Parkins, H. Shibuya, I. Cecic, M. R. Stratford and D. J. Chaplin (2000) Nitric oxide production by tumour tissue: impact on the response to photodynamic therapy. *Br. J. Cancer* **82**, 1835–1843.
50. Green, P. J. (1984) Iteratively reweighed least squares for maximum likelihood estimation, and some robust and resistant alternatives (with discussion). *J. R. Statist. Soc.* **46**, 149–192.
51. Koch, G. and S. Edwards (1988) Clinical efficacy trials with categorical data. In *Biopharmaceutical Statistics for Drug Development* (Edited by C. E. Peace), pp. 403–457. Marcel Dekker Press, New York.
52. McCullagh, P. (1980) Regression models for ordinal data. *J. R. Statist. Soc. B* **42**, 109–142.
53. Agresti, A. (1984) *Analysis of Ordinal Categorical Data*. John Wiley & Sons, New York.
54. Hosmer, D. W. and S. Lemeshow (1989) *Applied Logistic Regression*. John Wiley & Sons, New York.